Astron. Astrophys. 341, 264–274 (1999)

ASTRONOMY AND ASTROPHYSICS

Wavelength shifts of emission line profiles due to velocity fields in the solar corona

R. Ventura and D. Spadaro

Osservatorio Astrofisico di Catania, CNR-Gruppo Nazionale di Astronomia, UdR di Catania, Città Universitaria, Viale A.Doria 6, I-95125 Catania, Italy

Received 2 December 1997 / Accepted 29 April 1998

Abstract. We have investigated the dependence of the wavelength shift of the coronal emission line profiles on the line of sight velocity of the emitting plasma.

The results of our numerical calculations point out that, while the wavelength shift of the collisionally excited component of the line is related to the line of sight velocity by the usual formula for the Doppler effect, that of the resonantly scattered component also depends on the angle of scatter and on the angle between the velocity vector and the line of sight.

For the same outflow velocity, the absolute value of the resonantly scattered component shift is significantly smaller than that of the collisional component. Since both mechanisms generally contribute to the formation of a coronal line, we conclude that the results of this work should be taken into account when deducing line of sight velocities from the analysis of emission line profiles observed in the extended solar corona.

Key words: Sun: corona – solar wind – Sun: UV radiation

1. Introduction

The possibility of observing intensity and profile of EUV emission lines in the extended solar corona, particularly by the UltraViolet Coronagraph Spectrometer (UVCS) (Kohl et al. 1995) on board the space mission SOHO (Solar and Heliospheric Observatory) (Domingo et al. 1995), is giving a great opportunity for investigating the physical conditions in the regions where the solar wind originates (Antonucci et al. 1997a,b; Kohl et al. 1997a,b; Noci et al. 1997; Raymond et al. 1997). The analysis of these observational data is being carried on by means of diagnostic techniques which have been extensively described in several papers (e.g., Kohl & Withbroe 1982; Withbroe et al. 1982; Noci et al. 1987).

Some of the emission profiles, particularly those obtained during the observation of coronal mass ejections (CMEs) (Antonucci et al. 1997b; Ciaravella et al. 1997), exhibit significant shifts of the line peak with respect to the rest wavelength, and these can be used to determine the velocities along the line of sight of the extended corona during a mass ejection.

Send offprint requests to: rventura@alpha4.ct.atro.it

It is worthwhile to note, in this respect, that there are two principal mechanisms generally contributing to the formation of a coronal line:
- collisional excitation by electron impact;
- resonant scattering of chromospheric and inner corona photons by ions in the outer corona.

These mechanisms have been described in detail by Kohl & Withbroe (1982), Withbroe et al. (1982) and Noci et al. (1987).

In the case of the collisional excited component of a coronal line, the wavelength shift $\Delta\lambda$ is related to the line of sight velocity of the emitting plasma, $v_{l.o.s.}$, by the usual formula $\Delta\lambda = \frac{\lambda_0}{c} v_{l.o.s.}$, where λ_0 is the rest wavelength of the line and c is the speed of electromagnetic radiation *in vacuo*. As far as the resonantly scattered component is concerned, the resulting shift of the emission profile is also affected by the way in which the incident chromospheric profile overlaps the absorbing coronal one. This aspect has been discussed by Noci & Maccari (1998, this issue), who have derived an approximate analytic expression for the shift of the emission profile, showing that the shift does depend on the angles a) between the line of sight and the line segment connecting Sun centre to the elementary volume of emission, and b) between the velocity vector and the line of sight. Noci and Maccari assumed a Gaussian chromospheric profile and a Maxwellian velocity distribution for the scattering ions.

This paper is in connection with the work of Noci & Maccari (1998): we present here numerical calculations of a set of emission profiles of the H I Lyα (1215.67 Å) and O VI (1031.95 Å) lines obtained for elementary volumes of emission with directions to Sun centre and velocity vectors forming different angles with the line of sight. As in several previous papers (Spadaro & Ventura 1993; 1994a,b; 1996) we have taken into account both the resonant scattering and the collisional excitation contribution to the line formation. Moreover we adopted different values of outflow velocity, density and temperature for the coronal plasma.

It is worth noting that the calculation of the collisional contribution to the emissivity profiles gives a reference for the wavelength shift expected for a given line of sight velocity. Moreover, including it in the estimate of the total emissivity gives a more realistic simulation of the emission profiles produced by the expanding coronal plasma.

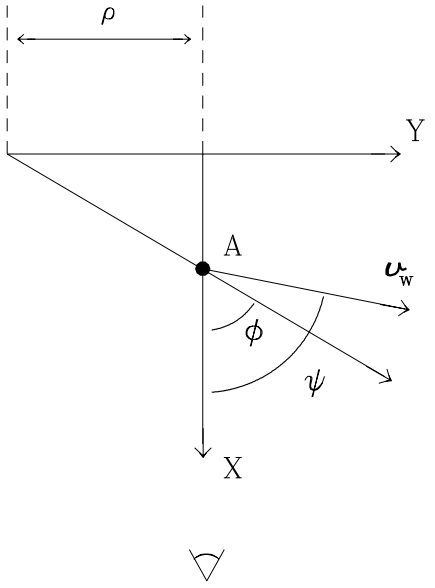

Fig. 1. Geometry adopted for calculation of the emission profiles from an elementary plasma volume located in A.

To complete our work, we have also calculated the Lyα intensity profiles, adopting a representative, simplified model of CME proposed by Steinolfson & Nakagawa (1977), integrating the emissivity of the various volume elements along the line of sight.

2. Theoretical treatment and numerical procedure

Fig. 1 illustrates the geometry adopted for calculating the emission profile from an elementary volume of plasma located in A. The X axis coincides with the line of sight while the Y axis connects the Sun centre to the point where the line of sight intersects the "plane of the sky" (i.e., the plane perpendicular to the line of sight which contains the Sun centre); ρ is the heliocentric distance of this point of intersection. The outflow velocity $\mathbf{v}_w$ lies on the XY plane, forming an angle ψ with the line of sight. ϕ is the angle between the direction from the Sun centre to A and the line of sight.

In the geometry described above the emissivity of the resonantly scattered component of a coronal spectral line is given by (e.g. Withbroe et al. 1982):

$$E_r(\lambda) = \text{const.}\, B_{12}\, \frac{A_{el}\, N_e R_i}{\lambda_0} \int_\omega p(\phi,\omega)\, d\omega \times \int_{-\infty}^{+\infty} I(\lambda^{'},\omega) d\lambda^{'} \int_{-\infty}^{+\infty} f(\mathbf{v}-\mathbf{v}_\mathrm{w}) \times \delta(\lambda^{'} - \lambda_0 - \frac{\lambda_0}{c}\,\mathbf{v}\cdot\mathbf{n}^{'}) \times \delta(\lambda_0 - \lambda + \frac{\lambda_0}{c}\,\mathbf{v}\cdot\mathbf{n})\, d(\mathbf{v}-\mathbf{v}_\mathrm{w}) \qquad (1)$$

where B_{12} is the Einstein coefficient for absorption, A_{el} is the elemental abundance, N_e the electron number density, R_i the ionization balance term of the emitting atoms (function of the plasma temperature) and λ_0 is the central wavelength of the transition. The angular dependence of the scattering process is described by the function $p(\phi,\omega)$, where ω is the solid angle under which the elementary volume of emitting plasma located in A subtends the solar disc.

$I(\lambda^{'},\omega)$ is the specific intensity of the chromospheric radiation at wavelength $\lambda^{'}$ and solid angle ω. $f(\mathbf{v}-\mathbf{v}_\mathrm{w})$ is the thermal velocity distribution function of the emitting atoms ($\mathbf{v}-\mathbf{v}_\mathrm{w}=\mathbf{v}_T$).

The first Dirac delta function takes into account that the only chromospheric photons incident on A from different directions (individuated by the unit vector $\mathbf{n}^{'}$ within the solid angle ω) which can be scattered by coronal atoms moving with a velocity $\mathbf{v}$ are those with $\lambda^{'} = \lambda_0 + \frac{\lambda_0}{c}\mathbf{v}\cdot\mathbf{n}^{'}$, the second Dirac delta function transforms the scattered wavelength from the atom's frame to the observer's frame; $\mathbf{n}$ is the unit vector parallel to the line of sight, directed toward the observer.

In our simulations we have assumed the lower atmosphere to be uniformly bright in the exciting radiation, which allows us to neglect the dependence on the solid angle ω of the chromospheric specific intensity $I(\lambda^{'},\omega)$, and adopted the *observed* intensities and profiles of the chromospheric exciting Lyα and OVI (λ 1031.95) lines reported respectively in Gouttebroze et al. (1978) and Noci et al. (1987). We also adopted a Maxwellian velocity distribution of the emitting ions which allows us to integrate analytically Eq. (1) over $\mathbf{v}_T$.

Expressing the velocity in dimensionless units: $\mathbf{u} = \mathbf{v}/\mathrm{w}$, where $\mathrm{w} = \frac{\lambda_0}{c}(\frac{2kT}{m})^{1/2}$ is the thermal Doppler width, and normalizing the wavelength shifts: $x = \frac{\lambda-\lambda_0}{\mathrm{w}}$ and $x^{'} = \frac{\lambda^{'}-\lambda_0}{\mathrm{w}}$, we

Table 1. Lyα line peak shifts (Å)

log v^a_{rad}	ϕ 90°	60°	30°	log v^b_{norad}	ϕ 90°	60°	30°
7.5				7.5			
	0.0	0.24	0.36		1.24	1.12	0.68
	0.0	0.64	1.12		1.28	1.28	1.28
	0.0	0.24	0.36		1.24	1.12	0.68
7.6				7.6			
	0.0	0.28	0.56		1.56	1.44	0.92
	0.0	0.80	1.40		1.60	1.60	1.60
	0.0	0.32	0.60		1.56	1.44	0.92
7.7				7.7			
	0.0	0.36	0.72		1.96	1.88	1.16
	0.0	1.00	1.76		2.04	2.04	2.04
	0.0	0.72	1.76		1.96	1.88	1.24
7.8				7.8			
	0.0	0.36	0.76		2.52	2.44	1.52
	0.0	1.28	2.20		2.56	2.56	2.56
	0 0	1.28	2.20		2.52	2.44	2.56

Note. We report for each considered value of velocity, from top to bottom, the absolute value of the wavelength shifts relative to the radiative, collisional and total emissivity profile, respectively.
[a] $\psi = \phi$
[b] $\psi = 0°$

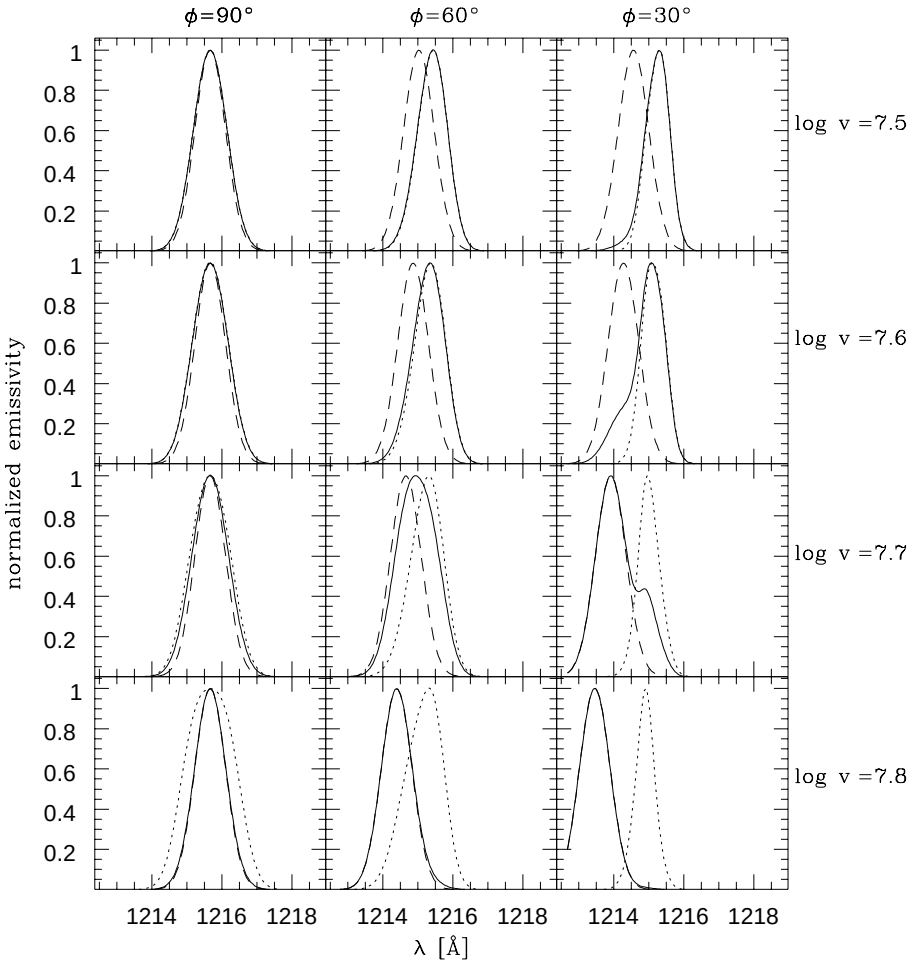

Fig. 2. Simulated Lyα emissivity profiles for radial outflow. Each panel reports the resonantly scattered component (dotted line), the collisionally excited component (dashed line) and the total line profile (solid line), each normalized to their own maximum value. From top to bottom we report the emissivity profiles obtained adopting increasing velocity values spanning, at equal step in the logarithm, the range log v (cm sec^{-1}) = [7.5 - 7.8]. For each considered value of velocity the three horizontal panels refer to the results obtained for $\phi = 90^\circ$, 60° and 30°, respectively.

obtained:

$$E_r(\lambda) \;=\; \mathrm{const.}\, B_{12}\, \frac{A_{el}\, N_e\, R_i}{\lambda_0} \int_{-\infty}^{+\infty} \int_{\omega} I(\lambda^{'})\, p(\phi,\omega) \times G_1(x, u_{\rm w}, \psi, \phi, \omega)\, G_2(x, x^{'}, u_{\rm w}, \psi, \phi, \omega)\, d\omega\, d\lambda^{'} \quad (2)$$

with

$$G_1 = \frac{\exp - [x + u_{\rm w} cos(\psi)]^2}{\pi {\rm w}^2 \beta^2} \qquad \text{and}$$

$$G_2 = \exp \frac{-[x^{'} - \alpha x + \beta u_{\rm w} sin(\psi)]^2}{\beta^2}$$

where $\alpha = \alpha(\phi, \omega)$ and $\beta = \beta(\phi, \omega)$ are the components of $\mathbf{n}^{'}$ in the X and Y directions, respectively.

The emissivity profile from a given elementary volume of plasma was then obtained numerically integrating Eq. (2) over ω and $\lambda^{'}$.

For the emissivity profile of the collisionally excited component we have used the expression (e.g. Withbroe et al. 1982):

$$E_c(\lambda) \;=\; \mathrm{const.}\, \lambda\, A_{el}\, R_i\, N_e^2\, C_{12}\, \Phi(\lambda) \quad (3)$$

where C_{12} is the collisional excitation rate coefficient and $\Phi(\lambda)$ the profile function which, under the adopted hypothesis of Maxwellian velocity distribution for the emitting ions, can be assumed to be Gaussian.

For more details and references on the adopted atomic data, elemental abundances and ionization balances we refer the reader to Spadaro & Ventura (1993, 1994a,b).

When an intensity profile was computed we integrated along the line of sight the emissivity contributions to the spectral intensity given by each elementary volume element.

3. Line emissivities

In order to perform the spectral line profile simulations presented here, we have chosen $\rho = 2R_\odot$ and considered three points with $\phi = 90^\circ, 60^\circ, 30^\circ$, respectively. For each point we have taken an outflow velocity either radial, i.e. $\psi = \phi$, or directed along the line of sight ($\psi = 0^\circ$), adopting in both cases the following values for the logarithm of the velocity (in cm s^{-1}): 7.5, 7.6, 7.7, 7.8. These high velocity values are selected in order to reproduce typical conditions for CME's. We assumed a value of 6.15 for the logarithm of the plasma temperature T (in K), and of 5.5 for that of the electron density N_e (in cm^{-3}).

Note that the adopted values for the angles ϕ and ψ produce only blue shifts of the line profiles. On the other side, if we consider a geometrical configuration symmetric with respect to the

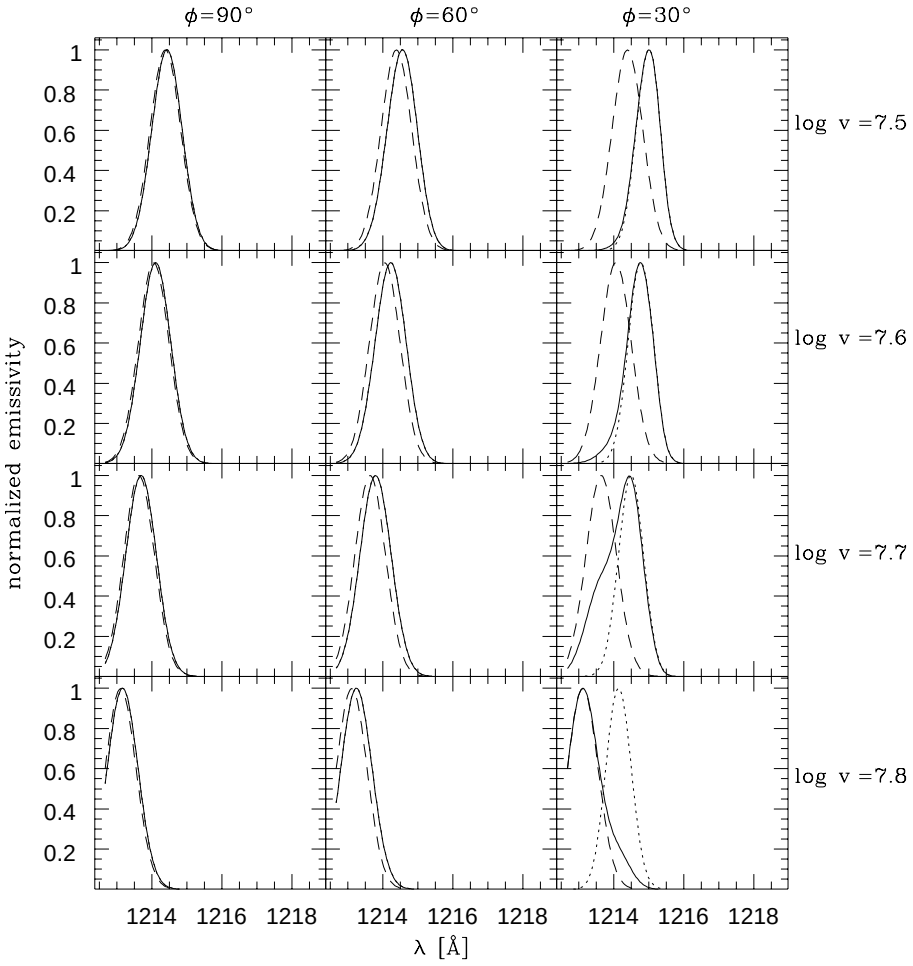

Fig. 3. As in Fig. 2, but for non-radial outflow ($\psi = 0°$).

"plane of the sky", i.e. taking the supplement of the angles ϕ and ψ chosen here, we obtain the same absolute value and opposite sign for the shifts of the profiles. Therefore the discussion of the results does not explicitly refer to the sign of the wavelength shifts, just to their absolute value.

The simulated Lyα emissivity profiles are reported in Figs. 2 and 3, for radial and non-radial outflow, respectively. They show that, for a non-null line of sight velocity and $\phi \neq 90°$, the wavelength shift of the resonantly scattered component is always significantly smaller than that of the collisional one (see also Table 1).

For radial outflows we note that the difference in the line peak shift exhibits an increase approximately proportional to the line of sight velocity, without a direct dependence on the angle $\phi = \psi$. In fact the only effect of varying ϕ, and then ψ, is to vary the component of the velocity along the line of sight. This is consistent with the formula given by Noci & Maccari (1998) for the wavelength shift of the resonantly scattered component of a line, when applied to a radial flow.

When we consider a non–radial flow, we note an increasing shift difference with decreasing ϕ. This is still in agreement with the expression of Noci and Maccari, if we take into account that in our calculations the angle ψ is constant and set equal to 0.

It is interesting to note that for each point on the Y axis and in the case of radial velocity ($\phi = 90°$) both the emissivity profiles have no shift of the line peak, but that of the resonantly scattered component becomes progressively wider than that of the collisional component as the outflow velocity increases.

Owing to the integration over the solid angle under which the scattering volume subtends the solar disc, the incident photons which do not come from the disc centre have directions forming angles with the line of sight different from $90°$. These photons give a contribution to the scattered profile shifted with respect to the rest wavelength of the line (see Noci & Maccari 1998). The absolute value of the shift increases with velocity. Since the angular distribution of the incident photons is symmetric around the Y axis, this results in a broadening of the scattered profile, whose width increases with outflow velocity.

We also note that the slightly smaller shift of the resonantly scattered profile with respect to the collisional one, found for a flow along the line of sight and $\phi = 90°$, can be attributed to the integration over the solid angle, because the incident photons with scattering angle different from $90°$ give a contribution to the scattered profile having a wavelength shift smaller than $\frac{\lambda_0}{c} v_{l.o.s.}$ (see Noci & Maccari 1998).

When we consider the total emissivity profile, obtained adding both the contributions from the resonantly scattered and

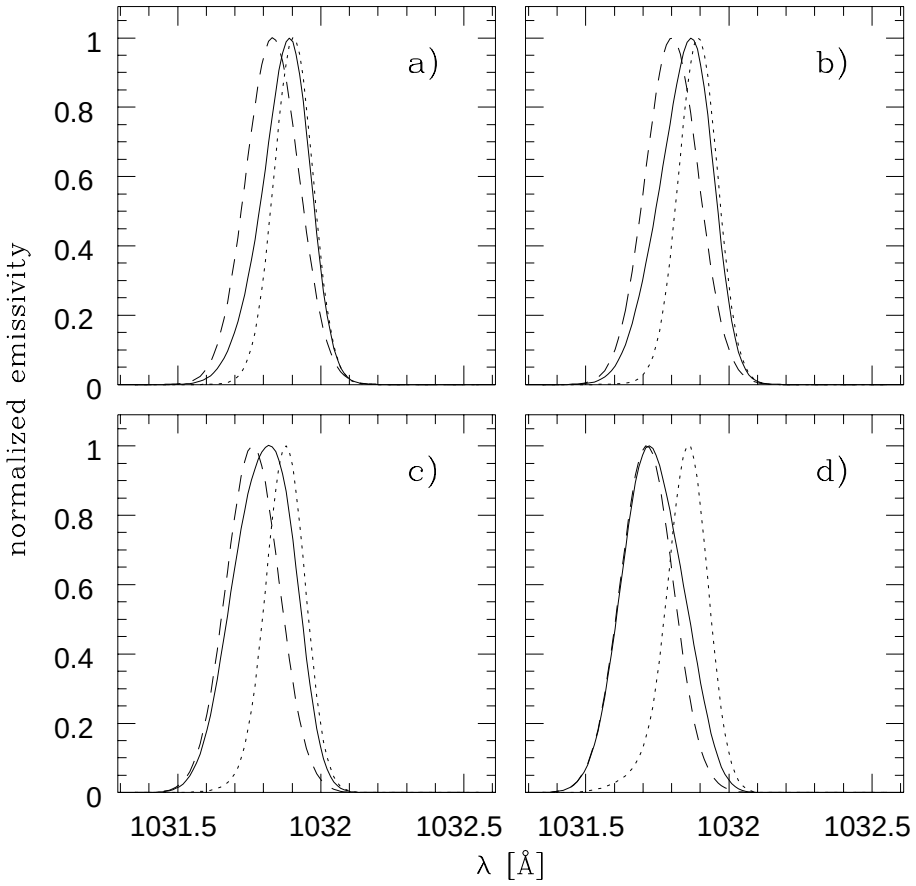

Fig. 4a–d. Simulated OVI (λ1031.95) emissivity profiles for radial outflow. In each panels we report the resonantly scattered component (dotted line), the collisionally excited component (dashed line) and the total emissivity profile (solid line), obtained setting the angle ϕ at 30° and adopting the following values of log v: 6.6 (**a**), 6.7 (**b**), 6.8 (**c**), 6.9 (**d**). The normalization to the unity has been carried out as in Fig. 2.

Table 2. Relative contributions (percent) of the resonantly scattered and collisional components to the total Lyα line emissivities for log N_e = 5.5, log T = 6.15 and different values of velocity and scattering angle

log v^a_{rad}	ϕ 90°	60°	30°	log v^b_{norad}	ϕ 90°	60°	30°
7.5				7.5			
	98	98	93		99	99	96
	2	2	7		1	1	4
7.6				7.6			
	94	92	75		99	99	90
	6	8	25		1	1	10
7.7				7.7			
	66	54	20		99	99	62
	34	46	80		1	1	38
7.8				7.8			
	6	3	1		99	99	11
	94	97	99		1	1	89

Note. We report for each considered value of velocity, from top to bottom, the relative contribution to the total emissivity of the radiative and collisional components, respectively.
[a] $\psi = \phi$
[b] $\psi = 0^\circ$

Table 3. Relative contributions (percent) of the resonantly scattered and collisional components to the total OVI (λ 1031.95) emissivities

log v^a_{rad}	rad. comp.	coll. comp.
6.6	57	43
6.7	47	53
6.8	33	67
6.9	16	84

[a] $\psi = \phi$

the collisional component, we note that for the lowest velocities ($\simeq$ 300 km/s) its shape and wavelength shift is essentially determined by the resonantly scattered profile. In fact the radiative contribution to the emission is still dominant (see Table 2). Note that for outflow velocities below 100 km/s it is more than two orders of magnitude higher than the collisional one (Withbroe et al. 1982).

The increase in the velocity component along the direction of the incident photons results in a less efficient scattering which produces a reduction of the resonantly scattered component owing to the relative shift of the coronal absorption line profile with respect to the chromospheric one. This effect is known as Doppler dimming (Hyder & Lites 1970; Beckers & Chipman 1974). Therefore the collisional component becomes more and more important in contributing to the shape of the line profile (see Table 2). In same cases, when the resonant component is

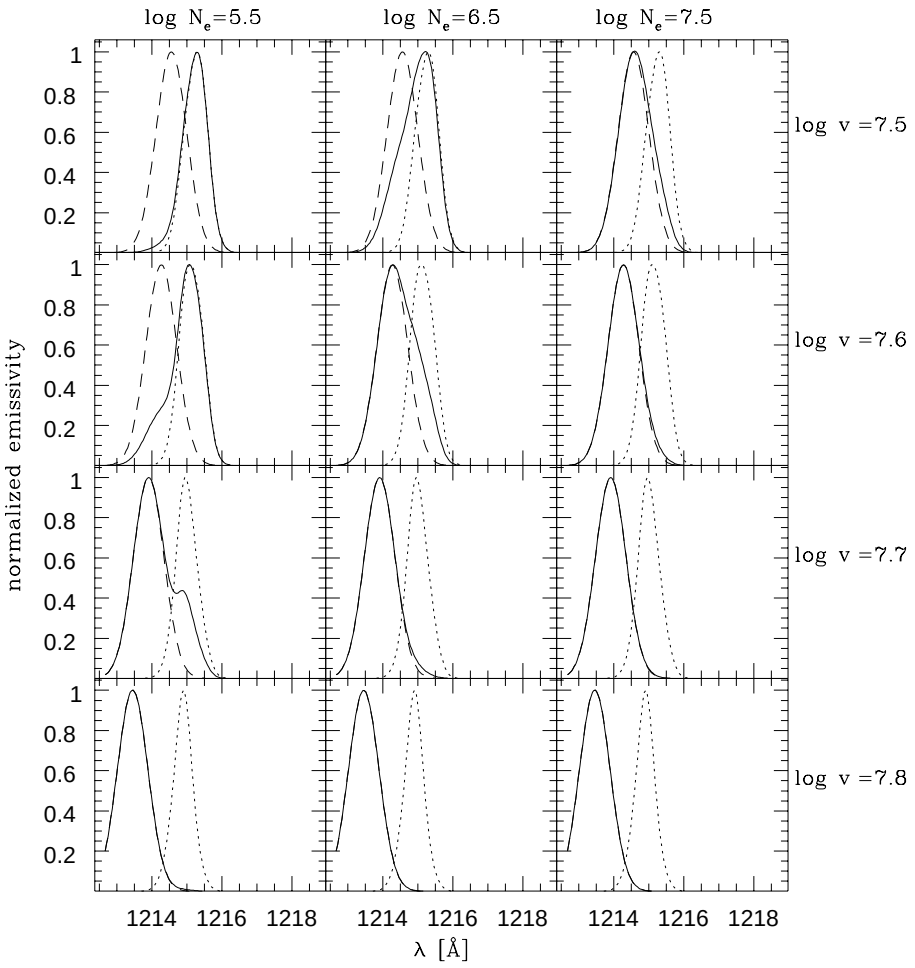

Fig. 5. Effect of plasma density on the Lyα emissivity profiles for radial outflow. Symbols and normalization are the same as in Fig. 2. The simulations reported have been obtained setting the angle ϕ at 30° and adopting increasing density values spanning, at equal step in the logarithm, the range log N_e (cm^{-3}) = [5.5 - 7.5]. Symbols, normalization and arrangement of the panels from top to bottom are the same as in Fig. 2.

considerably depleted by the outflow velocity, we can note that the total profile exhibits some asymmetries or even a splitting in two components. This could be useful if we wanted to consider separately the resonantly scattered and the collisional contributions to the line. When the velocity is sufficiently high to make the radiative component much lower than the collisional one, the total profile is essentially determined by the latter component and its shift is related to the line of sight velocity through the usual expression for $\Delta\lambda$.

It is worth noting that, for a given value of the flow velocity, the average component of the velocity along the direction of the incident photons is higher for radial than for non–radial outflows (see Fig. 1). Therefore the behaviour described above is slightly more evident in the first case.

As for the O VI line, the emissivity is already totally collisional at a velocity of $\simeq$ 300 km/s (log v = 7.5), because the radiative component is depleted very much by the Doppler dimming (see, e.g., Noci et al. 1987). At higher velocities the radiative component is even more Doppler dimmed.

Therefore, if we wish to put into evidence in the total emissivity profile the separation between the resonantly scattered and the collisional component, we have to consider lower velocities. The results of these calculations, obtained for flow velocities below 100 km/s, are shown in Fig. 4. In this case we can clearly note the different shifts obtained for the radiative and collisional components, in general agreement with the results found for the Lyα line, but they do not differ sufficiently to produce a marked splitting of the total emissivity profile. If we increase the velocity in order to have a larger Doppler shift difference between the two components, the steep decrease of the radiative component (Withbroe et al. 1982; Noci et al. 1987) yields a total emissivity profile completely dominated by the collisional component (see Table 3).

3.1. Effects of density, temperature and spectral distribution of the incident photons

Since the resonantly scattered and the collisional components of the line have different dependence on the plasma density, it is worthy to investigate the possible effect of density on the shape of the simulated emission profiles. Therefore, setting the angle ϕ at 30°, we have calculated the Lyα line profiles also taking an electron density one order and two orders of magnitude larger, leaving unchanged the plasma temperature. The behaviour of the simulated profiles for the radial outflow is shown in Fig. 5.

When we consider separately the resonantly scattered and collisional components, we note that the increase in density has no effect on their wavelength shift, as expected. However, while

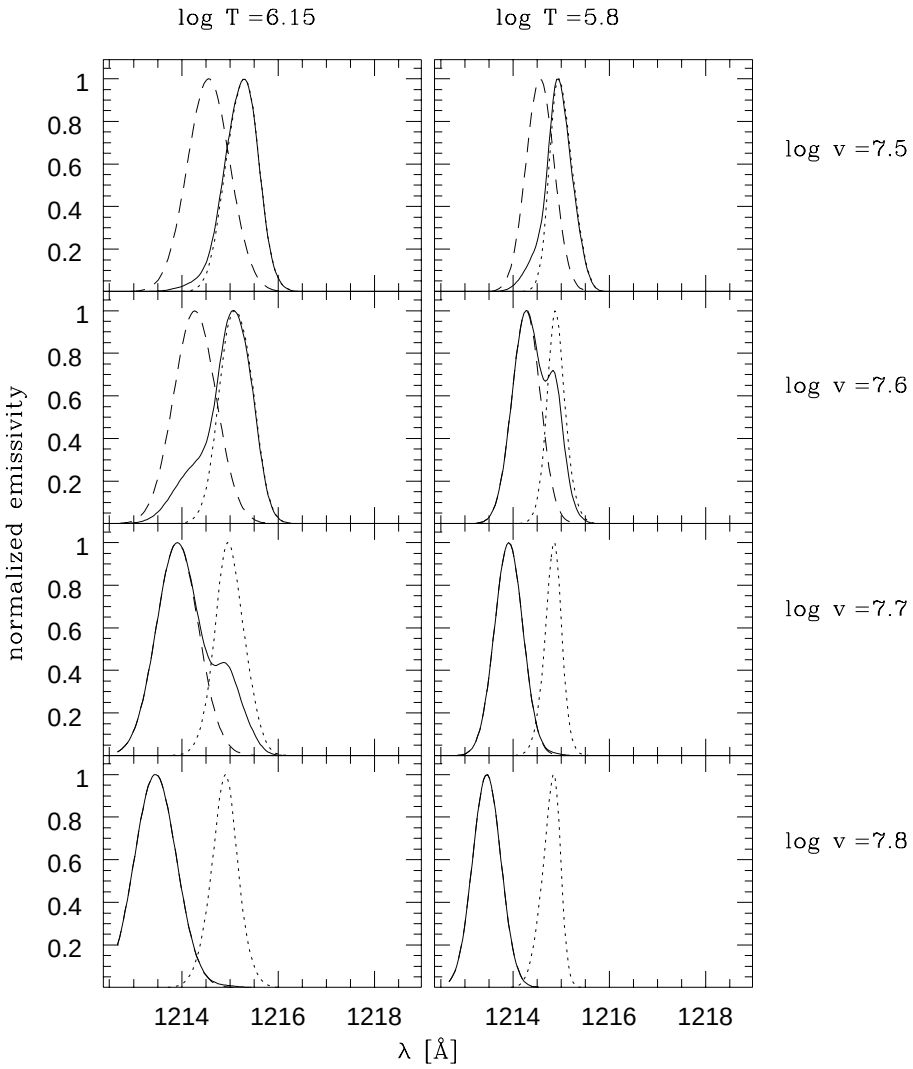

Fig. 6. Effect of temperature on the Lyα emissivity profiles for radial outflow. The simulations reported have been obtained setting the angle ϕ at 30° and log N_e (cm^{-3}) at 5.5, and adopting for the logarithm of T (K) the values 6.15 (left panels) and 5.8 (right panels). Symbols, normalization and arrangement of the panels from top to bottom are the same as in Fig. 2

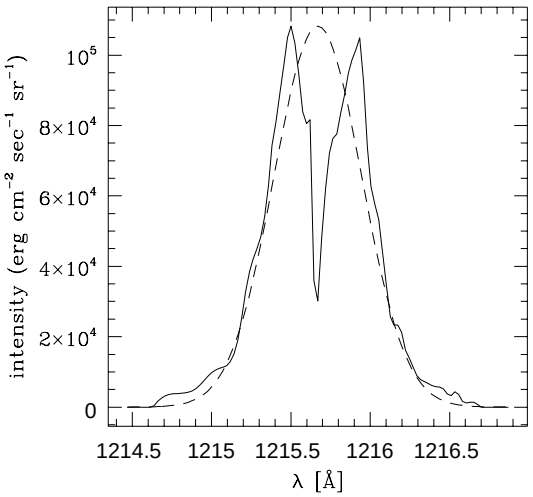

Fig. 7. Chromospheric Lyα profiles: observed (Gouttebroze et al. 1978) (solid line) and Gaussian (dashed line). The Gaussian profile has the same total intensity of the observed one and approximately the same 1/e width.

the former component depends simply on the density (see Eq. (1)), the latter one depends on the squared density (see Eq. (3)), so that it becomes more and more important in contributing to the shape of the total line profile, as the density increases for a given value of the outflow velocity (see Table 4).

This causes the total line profile to exhibit some asymmetries, until to be dominated by the collisional contribution, and its wavelength shift to be closer and closer to the value expected for the collisional component.

We find a similar behaviour also for the non–radial outflow.

We have also evaluated a possible effect of the temperature on the simulated Lyα results, considering a lower temperature value (log T = 5.8) for the coronal plasma and taking again the angle ϕ equal to 30° as well as the original value of the density (log N_e = 5.5). The results of this test for the radial outflow are shown in Fig. 6. Similar results are found for the non–radial flow.

First of all we notice that the line profiles are narrower, as an obvious consequence of assuming a lower temperature for the coronal plasma. We also note that while the wavelength shift of the collisionally excited component is unchanged, as ex-

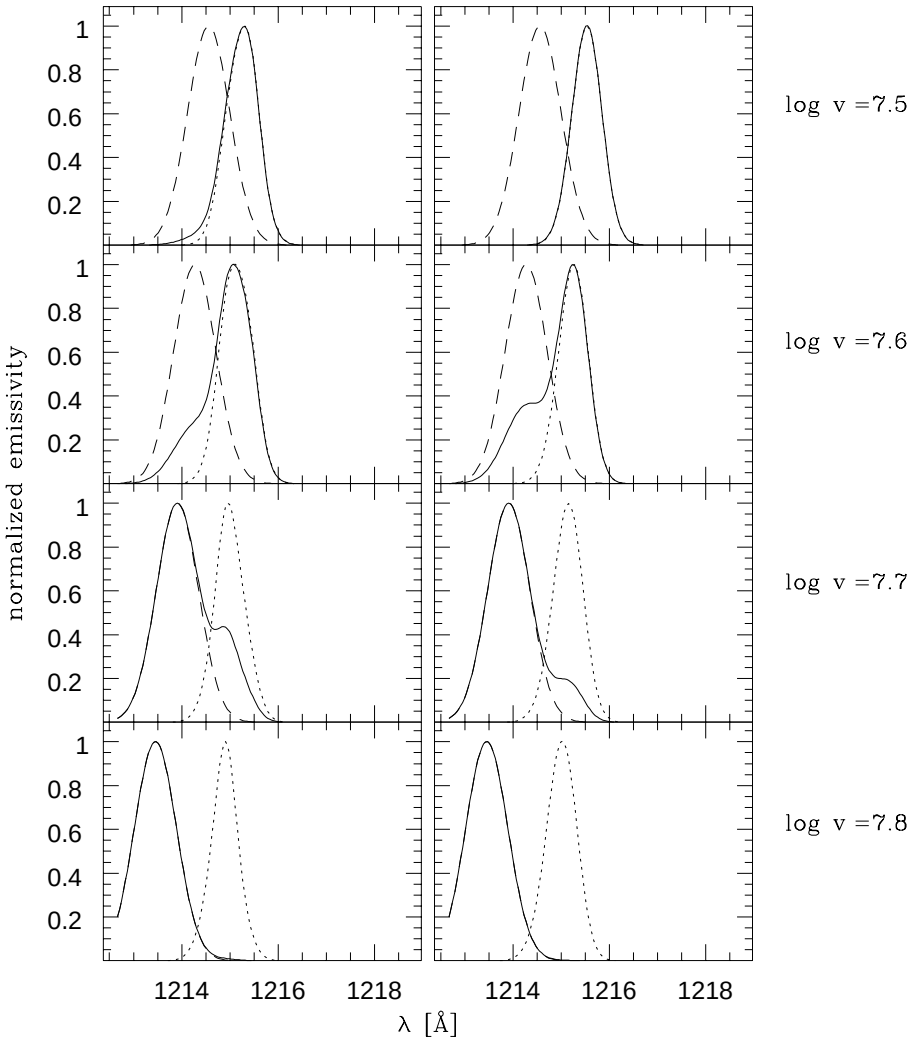

Fig. 8. Effect of the shape of the exciting chromospheric Lyα profiles on the coronal emission profiles for radial outflow. The simulations reported have been obtained setting the angle ϕ at 30°, log N_e (cm^{-3}) at 5.5 and log T (K) at 6.15 and adopting the two different chromospheric profiles shown in Fig. 7. Left panels refer to the emission coronal profiles obtained adopting the *observed* chromospheric profile; right panels refer to those obtained adopting the *constructed* Gaussian chromospheric profile. Symbols, normalization and arrangement of the panels, from top to bottom, are the same as in Fig. 2.

pected, the shift of the resonantly scattered component is larger than for higher temperatures. This result is consistent with the approximate analytical expression reported by Noci & Maccari (1998) for the shift of a line excited by resonant scattering, which gives, with the same width of the exciting chromospheric profile, a larger shift for a narrower width of the coronal absorption profile. In fact the assumption of a lower coronal temperature implies a narrower width of the coronal profile.

Cooling the plasma also results in a less efficient resonant scattering of chromospheric Lyα photons, due to the smaller extent of the overlapping between the chromospheric emission profile and the narrower coronal absorption profile. Consequently, the contribution of the collisional component to the total line profile becomes important at lower outflow velocities (see Table 4). For example, for log v = 7.6, the total profile calculated at log T = 6.15 is dominated by the resonantly scattered component and the collisional one only causes an asymmetry in the blue wing. At log T = 5.8, on the contrary, the total profile appears split, with the contribution from the collisional component significantly higher than that from the resonantly scattered one. Therefore, also the wavelength shift of the line peak is about 0.8 Å larger than in the former case.

Finally, we have investigated the effect of the shape of the exciting chromospheric profile on the resulting coronal emission profile. Fig. 7 reports the profile of the chromospheric Lyα line observed by Gouttebroze et al. (1978), used for calculating the resonantly scattered coronal profiles discussed above, as well as a Gaussian profile having the same total intensity and approximately the same $1/e$ width. Adopting the Gaussian exciting profile, we have calculated the resonantly scattered component profile of the Lyα for $\phi = 30°$, log N_e = 5.5 and log T = 6.15. The results for the radial outflow are shown in Fig. 8 (see also Table 4), and are analogous also for the non-radial flow.

It appears that the detailed shape of the exciting profile has some effect on the wavelength shift of the resonantly scattered profile, because it is slightly smaller when we adopt the Gaussian profile. In this case, also the total line profile has a smaller shift, at least at lower velocities.

Trying to explain this result, we note in Fig. 7 that the intensity distribution vs. wavelength of the line observed by Gouttebroze et al. (1978) makes it broader than the Gaussian line, particularly at higher intensities. Hence the ratio between the width of the incident profile and that of the coronal absorption one can be considered larger when we adopt the observed chro-

Table 4. Relative contributions (percent) of the resonantly scattered and collisional components to the total Lyα line emissivities for ϕ = 30° and different values of velocity, log N_e, log T and chromospheric exciting profiles

log v^a_{rad}	log T = 6.15 log N_e			log N_e = 5.5 log T		log N_e = 5.5 log T = 6.15	
	5.5	6.5	7.5	5.8	6.15	Gauss [b]	Observed [c]
7.5							
	93	58	12	80	93	99	93
	7	42	88	10	7	1	7
7.6							
	75	23	3	27	75	66	75
	25	77	97	73	25	34	25
7.7							
	20	3	0.2	0.5	20	11	20
	80	97	99.8	99.5	80	89	80
7.8							
	1	0.0	0.0	0.0	1	0.2	1
	99	100	100	100	99	99.8	99

Note. We report for each considered value of velocity, from top to bottom, the relative contribution to the total emissivity of the radiative and collisional components, respectively.
[a] $\psi = \phi$
[b] Gaussian exciting chromospheric profile.
[c] Observed chromospheric profile (Gouttebroze et al. 1978).

mospheric line. According to the expression of Noci & Maccari (1998), the shift of the coronal emission profile is larger when this ratio is larger, as it results from our calculations.

4. Line intensities from a simplified model of CME

We have modelled the coronal mass ejection as a cone, with the vertex in the centre of the Sun and an angular extent of 30 degrees. Within this region we have assumed radial symmetry, as well as radial plasma velocities. This geometry, while rather simple, is consistent with some white–light coronagraphic observations of CME's from space (Hundhausen, 1993). The values of plasma temperature, density and velocity used in the calculation of spectral line intensities are those derived by Steinolfson & Nakagawa (1977) in a study of the dynamical response of the solar corona induced by a transient energy input located near the coronal base, carried out adopting the spherically symmetric, single fluid, adiabatic model described in Nakagawa & Steinolfson (1976).

In our calculations, we have considered for the perturbed solar corona the radial profiles of the plasma parameters corresponding to the "base simulation" of Steinolfson and Nakagawa. These profiles, reported in Fig. 9, are calculated at a time t = 90 min after the perturbation has been introduced.

Fig. 10 reports the Lyα intensity profiles (resonantly scattered, collisional and total) obtained for different values of the heliocentric distance ρ and of the angle ϕ between the axis of symmetry of the simulated CME and the line of sight. In each examined case the line of sight intersects the axis of symmetry

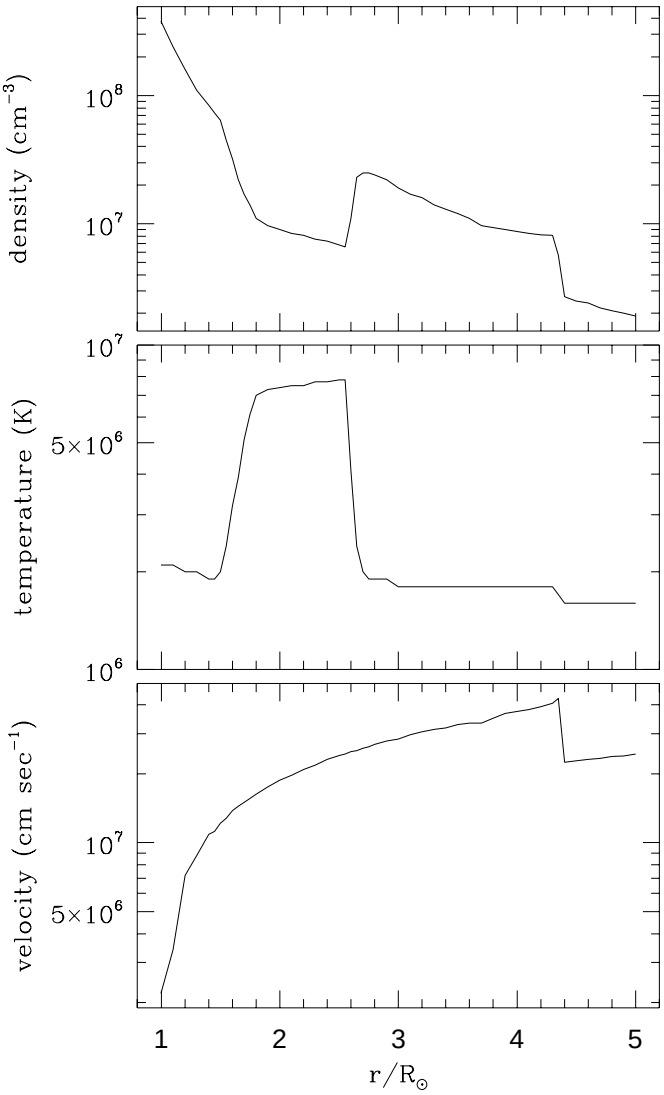

Fig. 9. Radial profiles of density (top), temperature (centre) and flow velocity (bottom) of the considered CME model (Steinolfson and Nakagawa, 1977).

in a point approximately coincident with the maximum outflow velocity (see the radial profile on the bottom of Fig. 9).

If the axis of symmetry lies in the "plane of the sky" ($\phi = 90°$), all the profiles are symmetric and centered on the rest wavelength, as a consequence of the radial symmetry assumed in the perturbed coronal regions.

For other orientations of the structure with respect to the line of sight, we note an evident difference in the wavelength shift (blue–shift) between the resonantly scattered component and the collisional one, with the shift of the latter component usually larger (in absolute value). This difference increases as the angle ϕ decreases.

Hence the behaviour of the intensity profile results are consistent with that of the emissivity profiles, even though integrating along the line of sight we add contributions from regions having different values of the physical parameters (see Fig. 9). Note that we have not taken into account in the present calcu-

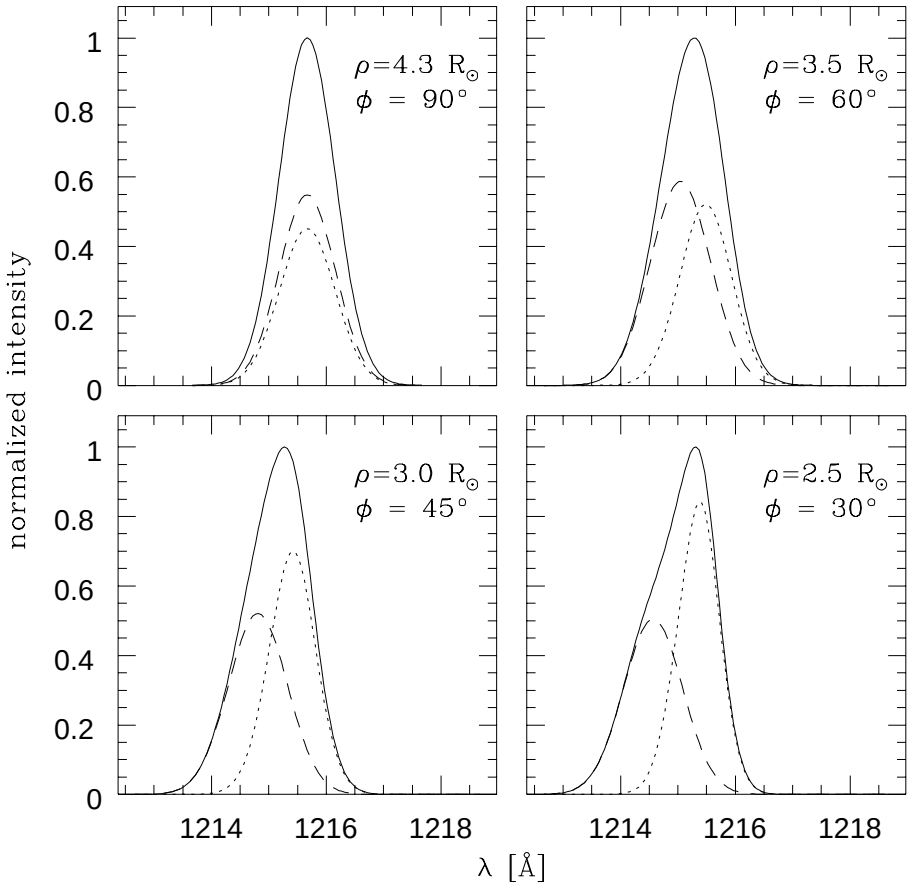

Fig. 10. Lyα intensity profiles for the adopted CME model. For each value of ρ and ϕ, the resonantly scattered (dotted line), collisionally excited (dashed line) components and total profiles (solid line) have been normalized to the corresponding total profile.

lations the contribution of the unperturbed corona surrounding the CME region. According to previuos simulations (Spadaro et al. 1994, Martin et al. 1997), this contribution should be negligible, without changing the behaviour of the simulated intensity profiles.

Also the total profile exhibits Doppler shifts with respect to the rest wavelength. Note that the resonantly scattered component progressively becomes more important in contributing to the shape and intensity of the total profile as the angle ϕ decreases. In fact the line of sight intersects regions of the perturbed corona with lower outflow velocities, so that the Doppler dimming is less effective in depleting the radiative component of the Lyα line. In each examined case, however, also the collisional component significantly contribute to the total line profile. For example, it causes the evident asymmetry on the profile blue side obtained for $\phi = 30°$.

5. Conclusions

The numerical calculations reported in this paper show that the wavelength shift of the emission line profiles observed in the extended solar corona may not depend simply on the line of sight velocity of the emitting plasma through the usual formula $\Delta\lambda = \frac{\lambda_0}{c} v_{l.o.s.}$. In fact, when the dominant contribution to the line emission is the resonant scattering of chromospheric and inner corona photons by ions in the outer corona, our simulations confirm the approximate analytic expression for the wavelength shift derived by Noci & Maccari (1998), putting into evidence the dependence of the shift on the angles a) between the line of sight and the line segment connecting Sun centre to the elementary volume of emission, and b) between the velocity vector and the line of sight. When the collisional excitation dominates the line emission, conversely, we find the usual dependence of the shift $\Delta\lambda$ on the line of sight velocity.

The wavelength shift of the emission profiles can also be affected by the density and temperature of the emitting plasma, as well as by the shape of the spectral distribution of the incident photons which excite the resonantly scattered component of the line.

Hence we conclude that this peculiar behaviour of the emission profiles in the extended solar corona must be taken into account when deducing line of sight velocities from the analysis of emission line profiles observed in the expanding outer corona.

As a concluding remark, it is worth noting the significant contribution of the collisionally excited component to the intensity of the Lyα line emitted by the extended corona during high outflow velocity events such as CME's. In fact this contribution, under the typical conditions of the expanding outer corona, is usually neglegible with respect to that of the resonantly scattered component which is about two orders of magnitude more intense (Withbroe et al. 1982). During a CME the collisional component can become significant for two reasons: first, the

radiative component is considerably depleted by the Doppler dimming caused by the high velocity outflow; second, these events are usually associated to an increase in the coronal density (e.g. Hildner et al. 1975; see also the plot on the top of Fig. 9). Therefore it cannot be neglected in the simulation of the Lyα emission from models of coronal mass ejections, in order to compare the modelled intensities to those observed during the occurrence of such events in the extended solar corona.

Acknowledgements. We wish to thank Ester Antonucci for suggesting this investigation. We also wish to thank the anonymous referee for useful suggestions which allows us to improve the description of the method and the results. This work has been supported in part by the Italian Ministero dell'Università e della Ricerca Scientifica e Tecnologica through the Astrophysical Observatory of Catania, the Agenzia Spaziale Italiana and the Gruppo Nazionale di Astronomia of C.N.R.

References

Antonucci E., Noci G., Kohl J.L. et al. 1997a, Proceedings of the Advances in Solar Physics Euroconference: Advances In the Physics of Sunspots. Tenerife, October 2 - 6, 1996. Astronomical Society of the Pacific, Conference Series 118, p. 273.
Antonucci E., Kohl J.L., Noci G. et al. 1997b, ApJ 490, L183.
Beckers J.M., Chipman E. 1974, Sol. Phys., 34 ,151.
Ciaravella A., Raymond J.C., Fineschi S. et al. 1997, ApJ 491, L59.
Domingo V., Fleck B., Poland A.I. 1995, Sol. Phys. 162, 1.
Gouttebroze P.,Lemaire P., Vial J.C., Artzner G. 1978, ApJ 225, 655.
Hildner E., Golsing J.T., MacQueen R.M. et al. 1975, Sol. Phys. 42, 163.
Hundhausen A.J. 1993, J. Geophys. Res. 98, 13177.
Hyder C.L., Lites B.W. 1970, Sol. Phys., 14, 147.
Kohl J.L., Withbroe G.L. 1982, ApJ, 256, 263.
Kohl J.L., Esser R., Gardner L.D. et al. 1995, Sol. Phys. 162, 313.
Kohl J.L, Noci G., Antonucci E. et al. 1997a, Adv.in Space Res. 20, No. 1, p. 3.
Kohl J.L., Noci G., Antonucci E. et al. 1997b, Sol. Phys. 175, 613.
Martin R., Maccari L., Noci G. 1997, Sol. Phys. 172, 215.
Nakagawa Y., Steinolfson R.S. 1976, ApJ 207, 296.
Noci G., Maccari L. 1998, A&A, submitted
Noci G., Kohl J.L., Withbroe G.L. 1987, ApJ, 315, 706.
Noci G., Kohl J.L., Antonucci E. et al. 1997, Adv. in Space Res. 20, No 12, p. 2219.
Raymond J.C., Kohl J.L., Noci G. et al. 1997, Sol. Phys. 175, 645.
Spadaro D., Ventura R. 1993, A&A, 276, 571.
Spadaro D., Ventura R. 1994a, A&A, 281, 245.
Spadaro D., Ventura R. 1994b, A&A, 289, 279.
Spadaro D., Ventura R. 1996, A&AS 115, 531.
Spadaro D., Ventura R., Martin R. 1994, Space Sci. Rev. 70, 365.
Steinolfson R.S., Nakagawa Y. 1977, ApJ 215, 345.
Withbroe G.L., Kohl J.L., Weiser H., Munro R.H. 1982, Space Sci. Rev., 33, 17.